Catalysis Today 176 (2011) 202–207

Contents lists available at ScienceDirect

Catalysis Today

journal homepage: www.elsevier.com/locate/cattod

Hydrodesulphurisation of 4,6-dimethyldibenzothiophene over NiMo catalysts supported on Ti(Al) modified MCM-41

Karolina Jaroszewska[a,*], Marek Lewandowski[b], Jolanta R. Grzechowiak[a], Bartłomiej Szyja[c]

[a] Wrocław University of Technology, Faculty of Chemistry, Gdańska 7/9, 50-340 Wrocław, Poland
[b] Centre of Polymer and Carbon Materials, Polish Academy of Science, 44-121 Gliwice, Sowińskiego 5, Poland
[c] Schuit Institute of Catalysis, Department of Chemical Engineering and Chemistry, Eindhoven University of Technology, Den Dolech 2, 5612 AZ Eindhoven, The Netherlands

ARTICLE INFO

Article history:
Received 30 September 2010
Received in revised form
29 December 2010
Accepted 4 January 2011
Available online 8 February 2011

Keywords:
TiMCM-41
AlMCM-41
Hydrodesulphurisation
4,6-Dimethyldibenzothiophene

ABSTRACT

Ti- and Al-containing MCM-41 materials, with a Si/M (M = Al(Ti)) molar ratio equal to 8, were used as supports for preparing NiMo HDS catalysts. On the surface of the MCM-41 based catalysts, agglomerations of the Mo oxo-species were observed. The incorporation of Ti and Al into the silica structure visibly enhanced the interactions between NiMo oxides phase and the mesoporous support. The results of 4,6-DMDBT HDS showed that the NiMo catalyst supported on TiMCM-41 was more efficient than that supported on Ti-free samples. From the distribution of 4,6-DMDBT HDS products we can conclude that over catalysts containing TiMCM-41 and SiMCM-41 the hydrogenation of DMBPh to MCHT occurs.

1. Introduction

Hydrodesulphurisation (HDS) is of considerable attention to the oil refining industry as the global environment becomes more concerned. Nowadays, much effort is made aimed at improvement of HDS catalysts in view of the most refractory sulphur compounds to desulphurise such as 4,6-dimethyldibenzothiophene (4,6-DMDBT). The results of HDS studies involving MCM-41 supported catalysts reported in the literature mainly refer to the desulphurisation of dibenzothiophene over catalysts prepared using AlMCM-41. The potential advantages of the use of modified mesoporous materials as a supports for hydrotreating catalysts are high surface area, porous system and medium acidity. The results of Silva-Rodrigo et al. [1] have shown the possibility of obtaining active NiMo HDS catalysts prepared with TiMCM-41. The NiMo/TiMCM-41 was found to display not only a higher activity in the HDS of thiophene but also a higher stability under hydrothermal conditions (600 °C) as compared to the NiMo/AlMCM-41. Thus, it would be of interest to investigate the activity of MCM-41 supported catalyst in HDS of the more refractory sulphur compounds such as 4,6-DMDBT, and this is the aim of the present study.

2. Experimental

A series of SiMCM-41, TiMCM-41 (Si/Ti = 8) and AlMCM-41 (Si/Al = 8) was obtained according to the procedure described elsewhere [2]. TiMCM-41 and AlMCM-41 were synthesized by direct hydrothermal method using titanium(IV) isopropoxide and aluminum(III) sulphate. The synthesis of TiMCM-41 was carried out in a dry glove-box filled with nitrogen. The detailed procedure for the formation of MCM-41 into pellets as well as preparation of NiMo catalysts supported on MCM-41 (14 wt.% MoO_3, 3 wt.% NiO) is provided in our previous work [3].

The XRD, N_2 sorption measurements have been described in [4,5]. TPR experiments were conducted in a flow system consisting of a quartz tube filled with about 0.2 g catalyst. The sample was heated up to 800 °C (10 °C/min) in flow of a mixture containing 10% (v/v) H_2 and 90% (v/v) Ar. The UV–vis diffuse reflectance spectra were recorded on Cary 100 Varian spectrophotometer. Catalytic activity was determined in HDS reaction of 4,6-DMDBT (300 ppm of sulphur in decalin) in a continuous-flow microreactor (350 °C, 6.0 MPa and contact time: 0.08–0.62 s). The catalyst (weight = 0.5 g, grain size 0.25–0.315 mm) was presulphided *in situ* with a mixture of 2.5% (V/V) dimethyldisulphide in decalin (350 °C, 6.0 MPa, 4 h). The reaction products were analyzed by GC method.

3. Results and discussion

The XRD patterns of SiMCM-41 and TiMCM-41 samples (Fig. 1a) confirmed a well-ordered structure for both types of materials. In

* Corresponding author. Tel.: +48 713206582; fax: +48 713221580.
E-mail address: karolina.jaroszewska@pwr.wroc.pl (K. Jaroszewska).

0920-5861/$ – see front matter © 2011 Elsevier B.V. All rights reserved.
doi:10.1016/j.cattod.2011.01.013

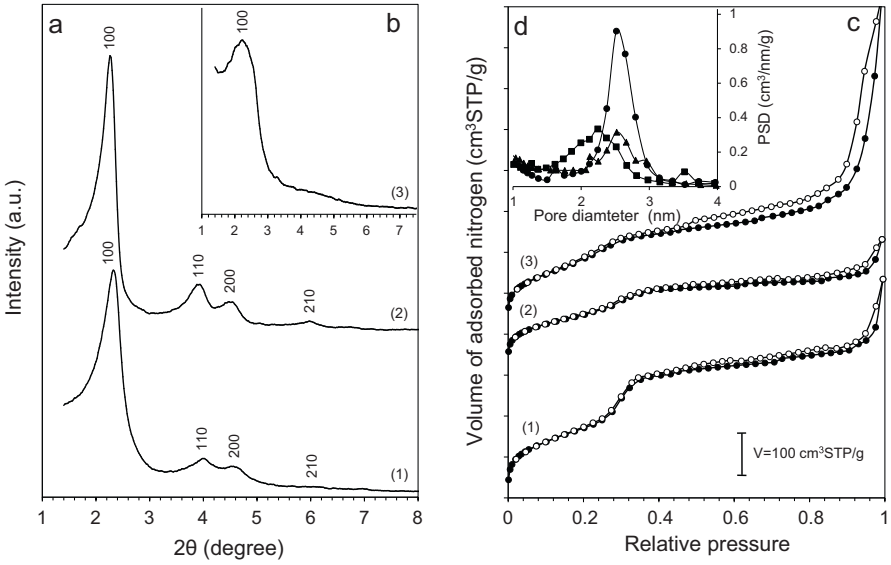

Fig. 1. Structure of the calcined MCM-41 samples: (a and b) XRD spectra and (c) nitrogen adsorption isotherms (denotation of the samples: (1) SiMCM-41, (2) TiMCM-41 and (3) AlMCM-41); (d) pore size distribution calculated using the BJH method (denotation of the samples: (●) SiMCM-41, (▲) TiMCM-41 and (■) AlMCM-41).

the case of AlMCM-41 (Fig. 1b) the X-ray diffractogram shows that the framework structure is partly disordered under the influence of Al incorporated species.

The N_2 sorption isotherms of the investigated MCM-41 samples exhibit a type IV isotherm (Fig. 1c). A steep capillary condensation step ($p/p_0 = 0.20–0.32$) is observed for SiMCM-41, suggesting a uniform-size pore system [6]. However, the step is gradually flat upon Ti and Al incorporation into the MCM-41 structure. Hysteresis of type H3 can be observed on AlMCM-41 sample above the relative pressure of 0.45, which is attributed to the capillary condensation of the nitrogen within interparticles and/or some impurity phases (e.g. aluminium oxide phase). As can be seen from Fig. 1d, SiMCM-41 sample has a narrow distribution of pores peak positions at 2.5 nm. In the case of TiMCM-41 as well as AlMCM-41 the main peak of pore size distribution (PSD) is somewhat broad and the curves show that, in addition to main size of pores (in 2.5 nm and 2.2 nm, respectively), there are contributions located at 3.0 and 2.2 nm for TiMCM-41 as well as at 3.6 and 1.3 nm for AlMCM-41. This suggests a partial destruction of the pore arrangement and the existence of some amorphous domains in the Ti and Al containing carriers.

The textural properties of the MCM-41 samples reveal that TiMCM-41 compared with SiMCM-41 and AlMCM-41 samples has lower S_{BET}, lower pore volume and thicker walls (Table 1). Results show a small shift to higher values of unit cell parameter and interplanar distance due to the presence of Al and Ti in the MCM-41 relative to the silica sample; it could be an indication that metals have been incorporated into framework of the sieve. On the other hand, the results of UV–vis for TiMCM-41 and ^{27}Al MAS NMR for AlMCM-41 (both not shown here) reveal that metals were incorporated partly into the extra framework positions. The altogether results confirmed that the incorporation of Ti and Al into MCM-41 causes deterioration of the structure that is more significant for AlMCM-41.

The TPR results for NiMo/MCM-41 catalysts are shown in Fig. 2a. The TPR profile of NiMo/SiMCM-41 exhibits strong low-temperature peak with maximum at 480 °C and the one of NiMo/TiMCM-41 display one broad peak at about 490 °C. In the case of AlMCM-41 containing catalyst the TPR run presents two peaks: at 556 and at 735 °C. According to the literature data [7] the low temperature peaks (400–600 °C) correspond with the first step of reduction of polymeric octahedral Mo species ($Mo^{6+} \rightarrow Mo^{4+}$), weakly bonded to the support surface (probably aggregates of MoO_3). As for all catalysts, the maximum of the main peak is associated with the reduction of both Mo species and Ni species (overlapping of MoO_3 and NiO reduction regions). It is worth noting that first reduction peak may be overlapped also with reduction of a $NiMoO_4$-like phase (main peak at 475 °C [8]). The high temperature peaks (above 600 °C) can be linked with the second step of the reduction of octahedral polymolybdates ($Mo^{4+} \rightarrow Mo^0$), as well as of the reduction of isolated tetrahedral Mo species ($Mo^{6+} \rightarrow Mo^0$) in strong interaction with the carrier [7].

The TPR results of NiMo catalysts reveal that Ti and Al incorporation leads to an increase in the temperature of Ni and Mo oxides reduction because of their stronger interaction with modified MCM-41. Attention should be given to the fact that the TPR runs of Al- and Ti-modified catalysts display lower main reduction peak than that of the pure silica one. Additionally, the peaks are broad and asymmetric. According to Klimova et al. [9], the broadening in low temperature peak can be an evidence that monolayer-type Mo dispersion (or close to monolayer) on the support is present. This means that the use of TiMCM-41 and AlMCM-41 as a support accounts for the increase in the relative amount of Mo species, which are the most dispersed on the support surface. The promoting effect of Ti and Al on the dispersion of Mo species was also described elsewhere [10,11]. The reduction peak for NiMo/AlMCM-41 at 735 °C suggests that tetrahedrally coordinated Mo species are interacting with Al species of the support forming $Al_2(MoO_4)_3$-like phase [11].

The UV–vis spectra of the supported NiMo samples are shown in Fig. 2b. All supported NiMo catalysts show absorption bands at 215, 270 and 330 nm. As reported elsewhere [12], the absorption bands in 200–230 nm are assigned to the both isolated molybdate (tetrahedral, MoO_4^{2-}) and polymolybdate (octahedral, Mo^{6+}) species, while in 260–280 nm are associated with the charge transfer transitions in polymolybdate species. The spectra of samples studied show a predominated band centred around 270 nm; that band is the most intense for NiMo/TiMCM-41 catalyst. It seems that Ti addition to the MCM-41 leads to an increase in the proportion of octahedral Mo species. The UV–vis results also show the highest relative amount of tetrahedral Mo species over AlMCM-41 surface. As for all the catalysts a small band appears in 320–340 nm. It has been clearly stated by Salerno et al. [13] that the $NiMoO_4$ phase possessing only octahedrally coordinated Mo and Ni species dis-

Table 1
Structural properties of synthesized mesoporous materials.

Sample	a_0 (nm)	d_{100} (nm)	h_w (nm)	w_d (nm)	V_p (m^3/g)	V_t (m^3/g)	S_{BET} (m^2/g)
SiMCM-41	4.40	3.81	1.18	3.22	0.43	0.54	704.3
TiMCM-41	4.51	3.91	1.65	2.86	0.26	0.35	540.1
AlMCM-41	4.59	3.98	[a]	[a]	[a]	0.46	770.0

a_0: distance between pore centres, $a_0 = 2d_{100}3^{1/2}$, d_{100}: interplanar spacing, h_w: pore wall thickness calculated using $h_w = a_0 - w_d$, w_d: primary mesopore size calculated using $w_d = cd_{100}[\rho V_p/(1 + \rho V_p)]^{1/2}$, V_p: primary mesopore volume determined using α_s-plot method, V_t: total pore volume, S_{BET}: specific surface area, p_{BET}/p_0: relative pressure range used in the BET method.

[a] Not estimated due to the lack of a linear high-pressure part of the α_s-plot and very broad X-ray diffraction peak.

play strong absorption band near 330 nm. The deconvolution (not shown) of the spectra in the UV region reveals that the proportion of $NiMoO_4$ phase exposed on the NiMo/TiMCM-41 (~26%) sample is larger than on the NiMo/SiMCM-41 (~14%) and NiMo/AlMCM-41 (~9%) samples. This finding gives evidence that the $NiMoO_4$ species (which can be a precursor to the formation of NiMoS active phase) are the most stabilized on the TiMCM-41 supported catalyst.

The UV–vis spectra of Ni^{2+} ions are shown in Fig. 2c. The absorption bands at 380, 430 and 720 nm are assigned to octahedral Ni species [14], whereas the absorption band at 580 nm corresponds to Ni species in tetrahedral symmetry [15]. The further one is asso-

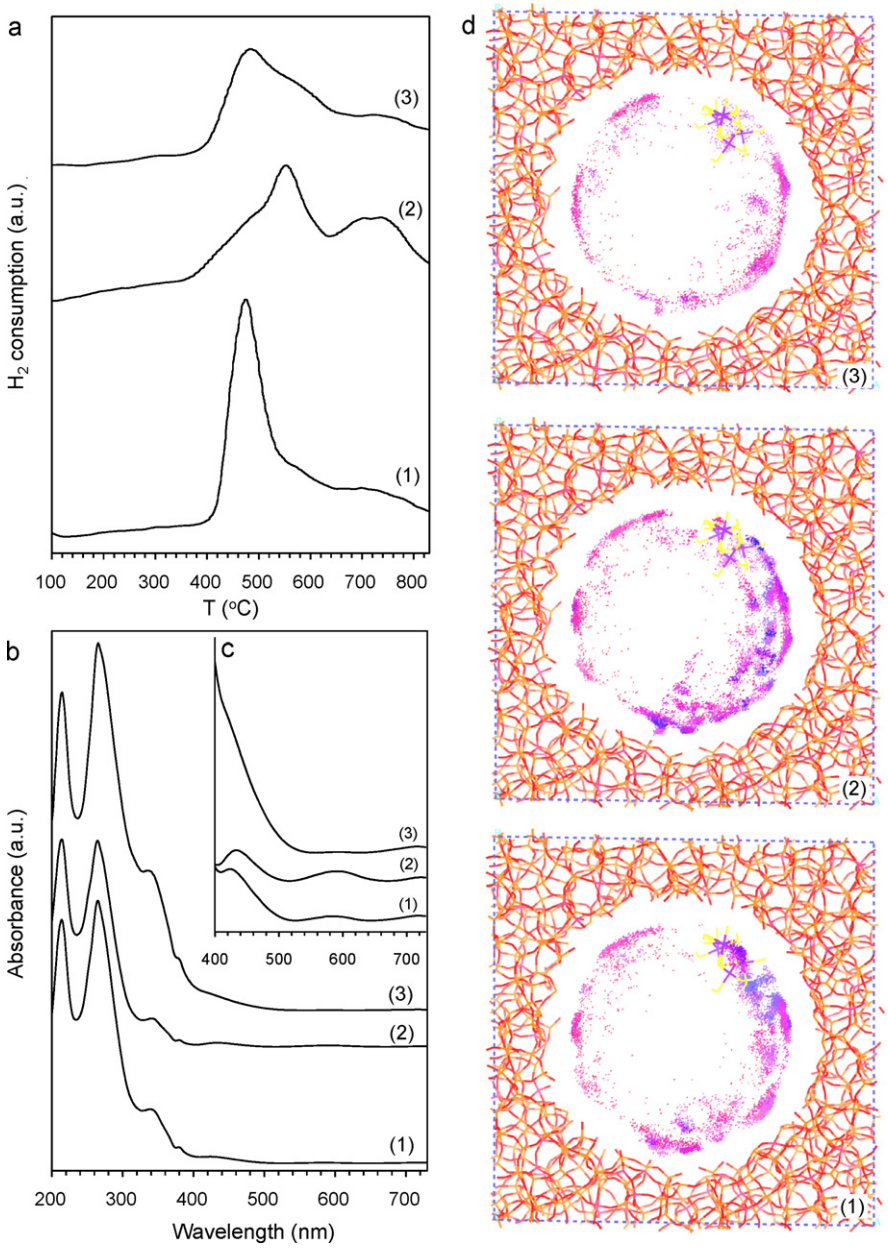

Fig. 2. Characterisation of NiMo MCM-41-based catalysts: (a) TPR profiles; (b and c) UV–vis spectra (denotation of the catalysts: (1) NiMo/SiMCM-41, (2) NiMo/AlMCM-41, (3) NiMo/TiMCM-41); (d) mass distribution of 4,6-DMDBT in the (1) MoS2/SiMCM-41, (2) MoS2/AlMCM-41 and (3) MoS2/TiMCM-41 models.

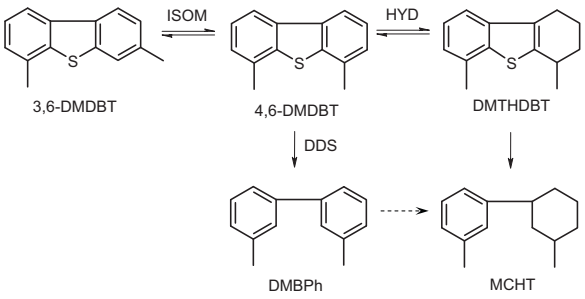

Scheme 1. Reaction network of the HDS of 4,6-DMDBT over MCM-41-based NiMo catalysts. *Hydrogenation of DMBPh to MCHT was observed over NiMo/SiMCM-41 and NiMo/TiMCM-41 catalysts.

ciated with the presence of characteristic of Ni species in a distorted spinel-like structure and it is predominant for NiMo/AlMCM-41 catalyst [13].

The activity of investigated catalysts was examined in the HDS of 4,6-DMDBT (Table 2). TiMCM-41 and SiMCM41 containing catalysts are more active than the catalyst supported on AlMCM-41. The HDS of 4,6-DMDBT changes with decreasing contact time from about 90 to 40% for NiMo/TiMCM-41 and NiMo/SiMCM-41 while only from 70 to 14% for NiMo/AlMCM-41. The hydrodesulphurisation reaction was found to be pseudo-first order with respect to 4,6-DMDBT (Fig. 3a). The rate constant values calculated for AlMCM-41 based catalyst is 1.78 and 1.47 times lower than for TiMCM-41 and SiMCM-41 containing catalysts, respectively. NiMo/AlMCM-41 is expected to display a higher activity than NiMo/SiMCM-41. Despite of the incorporation of Al into the support provides a stronger metal–support interaction, allowing an improved dispersion of the Mo and Ni oxides, lower activity of NiMo/AlMCM-41 (as compared to NiMo/SiMCM-41) can be associated with too strong metal–support interaction. Formation of $Al_2(MoO_4)_3$ and nickel distorted spinel-like structure makes the reduction and sulphidation of Ni and Mo species more difficult.

Our results show that the incorporation of Ti into the MCM-41 framework increases the activity of the NiMo catalysts as compared to the Ti-free catalysts. This can be attributed to the higher stability of $NiMoO_4$ phase over the TiMCM-41 surface.

It is well known from the literature that hydrodesulphurisation of 4,6-DMDBT on sulphide catalysts occurs through two parallel reactions: (i) direct desulphurisation (DDS) yielding 3,3′-dimethylbiphenyl (DMBPh) and (ii) hydrogenation with subsequent desulphurisation (HYD), yielding first tetrahydro-, hexahydro- and decahydro-intermediates of DMDBT (designated DMTHDBT, DMHHDBT, and DMDHDBT, respectively) and then 3-(3′-methylcyclohexyl)-toluene (MCHT) and 1-methyl-3-(3-methylcyclohexyl)cyclohexane (designated 3,3-dimethylbicyclohexyl DMBCH). With bifunctional catalysts there is commonly observed hydrocracking reactions yielding toluene and methylcyclohexane as well as isomerisation of 4,6-DMDBT yielding 3,6-dimethyldibezothiophene (3,6-DMDBT). In the present study the main products are: DMBPh, MCHT, DMTHDBT and traces of 3,6-DMDBT. These are presented in Scheme 1, with all sulphur-containing compounds on the top horizontal line and the final hydrocarbon products on the bottom line.

The results show that at the contact time in the range of 0.08–0.31 s for all the catalysts there is no preferential pathway in 4,6-DMDBT HDS. However, at $\tau = 0.62$ s the HYD/DDS activity of the catalysts can be ordered as follows:

$$\text{NiMo/TiMCM-41}(2.42) >, \text{NiMo/SiMCM-41}(2.36) > \text{NiMo/AlMCM-41}(1.01)$$

From the product distribution curves (Fig. 3b–d) for all the catalysts, we can see that the MCHT yield increases with increasing contact time. When AlMCM-41 was used as catalyst support, the rise in the DMBPh yield is observed. With NiMo/TiMCM-41 and NiMo/SiMCM-41 catalysts, the yield of the DMBPh reaches the highest value at the 0.31 s and then starts to decrease. This finding suggests that some part of the DMBPh which forms via DDS undergoes hydrogenation to MCHT. But this contradicts the results obtained for the $NiMo/Al_2O_3$ catalysts [16], which show that DMBPh does not undergo hydrogenation to MCHT.

One way to improve the 4,6-DMDBT HDS efficiency is the increase of hydrogenating function of the catalyst. In our study, the Grand Canonical Monte-Carlo (GCMC) molecular modelling method was used to carry out simulations of the adsorption of 4,6-DMDBT as well as DMTHDBT (the intermediate product of the 4,6-DMDBT hydrogenation) on the surface of the model. This is well developed method, which has been used for many years in order to study the adsorption phenomenon [17]. For the needs of this work we have used amorphous SiO_2 model as the initial geometry, on which all models are based. The model of each catalyst had a cubic shape with the cell dimensions of 3 nm. In the centre of this model, along the axis z we have formed a cylindrical shaped mesopore of 2 nm diameter, and length equal to the side of the unit cell. The MoS_2 cluster was adopted as the active phase for HDS catalysts. The chemical composition of the Al- and Ti-containing models have been obtained by substitution selected Si atoms by metals (Si/M ratio was equal to 8). The calculations of adsorption have been carried out for 327 °C and 2 kPa.

The adsorption isotherms of 4,6-DMDBT and DMTHDBT (not shown) demonstrate that the number of adsorbed molecules depends on the chemical composition of the catalysts. MoS_2/SiMCM-41 and MoS_2/AlMCM-41 display similar adsorptive properties with respect to both: 4,6-DMDBT and DMTHDBT molecules. The biggest difference can be seen for MoS_2/TiMCM-41; while the adsorption of 4,6-DMDBT is the weakest, the number of DMTHDBT molecules is the biggest. That means, that DMTHDBT (intermediate species in the HDS reaction) blocks the adsorption centres of the catalyst, preventing 4,6-DMDBT to be adsorbed. This is the example of competitive adsorption between the reagents of the process. The results of simulation with respect to the competitive adsorption stand in contradiction with experimental data (the activity of NiMo/TiMCM-41 is greater than others). Therefore, we have to conclude, that there are other factors responsible for the catalytic activity, such as discussed differences in the metal–support interactions.

Fig. 2d shows the mass distributions of the 4,6-DMDBT; each dot indicates the centre of the molecule mass. As all the calculated interactions energies are negative, all reactant molecules are attracted to the surface, however, the intensity of the interaction is different for the reactants and the model of the catalysts. These intensities are represented by the colour of the dot – from the lowest energy (the strongest interaction) which is shown as blue, through the shades of purple and pink, to the highest energy (the weakest interaction) which is represented by the red colour. In the case of 4,6-DMDBT adsorption on MoS_2/TiMCM-41, reactants only form a monolayer at the surface (Fig. 2d(3)). This fact is also related to the adsorption isotherm discussed above (the low number of 4,6-DMDBT molecules). The homogeneous distribution of dots means that the adsorption centres are located close to each other, and the energy of interaction is very similar for all those places. This is caused by rapid and easy translation of reactants between the adsorption centres. In the case of Ti-free samples the distribution of mass is less homogeneous and therefore specific adsorption centres are being formed. Moreover, as the number of molecules is increasing, the available space at the surface is reduced, and the only option is to adsorb in the second layer, close to the centre of

Table 2
4,6-DMDBT conversions and reaction product compositions obtained over NiMo MCM-41-based catalysts.

	[a]k_{HDS} (s^{-1})	τ (s)	Conv. (%)[b]	HDS (%)[c]	HYD/DDS[d]
NiMo/SiMCM-41	3.73	0.62	91.4	90.6	2.36
		0.31	72.4	70.6	0.98
		0.21	65.1	63.1	0.90
		0.15	58.3	55.9	0.86
		0.08	42.5	39.6	0.78
		0.62[e]	87.4	86.6	1.16
NiMo/AlMCM-41	2.26	0.62	75.4	71.9	1.01
		0.31	49.0	43.6	0.98
		0.21	35.7	30.4	0.97
		0.15	26.2	21.1	1.03
		0.08	18.0	13.6	1.00
NiMo/TiMCM-41	4.04	0.62	93.0	92.3	2.42
		0.31	73.2	71.2	1.20
		0.21	62.8	60.0	1.07
		0.15	52.9	49.8	0.98
		0.08	48.4	45.2	1.14

[a] kHDS: calculated from a pseudo first order global law.
[b] Total conversion of 4,6-DMDBT.
[c] Conversion of 4,6-DMDBT towards products without sulphur atom (DMBPh, MCHT).
[d] HYD/DDS ratio was determined as the ration of HYD route products (MCHT and DMTHDBT) to DDS route product (DMBPh).
[e] Data obtained after 40 h reaction time.

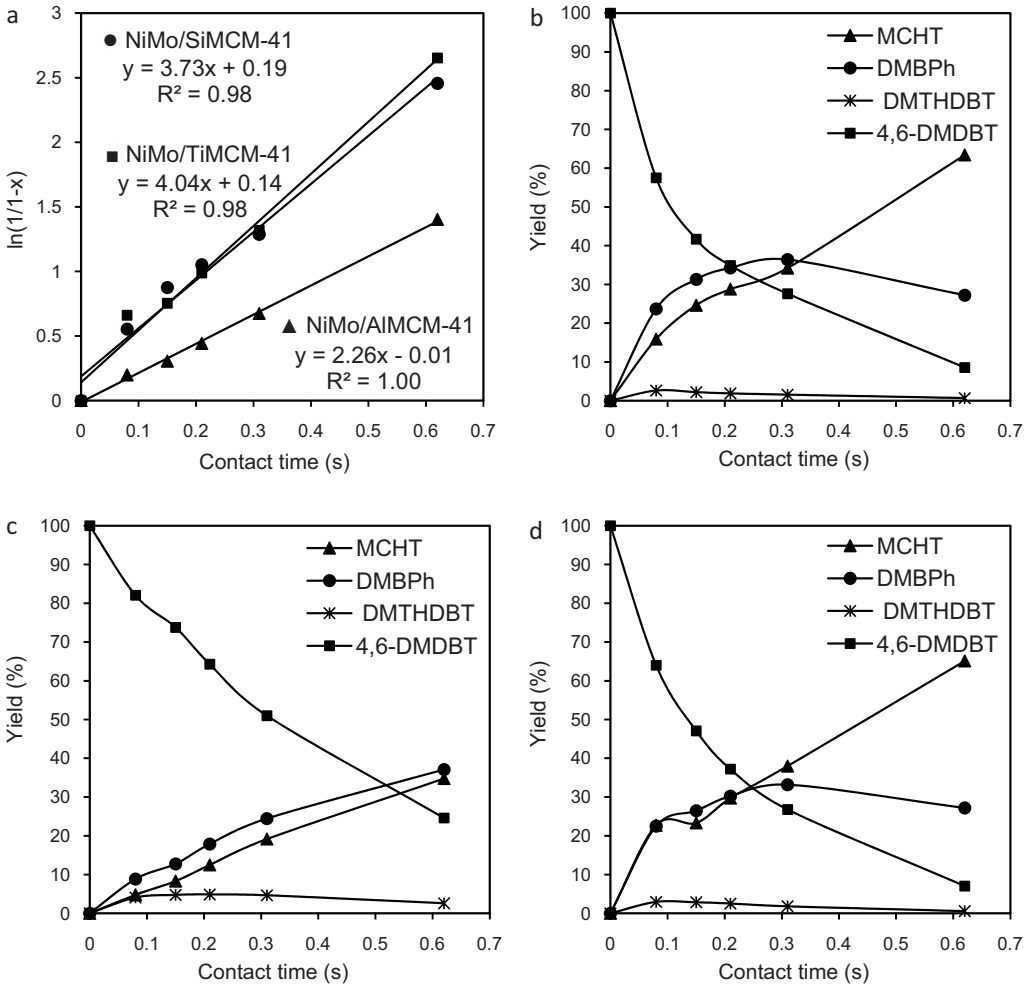

Fig. 3. $\ln(1/1-x)$ vs. contact time where x is the 4,6-DMDBT global conversion (a) and distribution of 4,6-DMDBT, intermediates and products observed during the HDS of 4,6-DMDBT over MCM-41-based catalysts: NiMo/SiMCM-41 (b), NiMo/AlMCM-41 (c) and NiMo/TiMCM-41 (d).

the pore. The results indicate that the chemical composition of the support influences the differences in adsorption.

4. Conclusions

According to the above results, the following conclusions can be stated:

1. The silica substitution by Ti and Al enhances the interactions between Ni and Mo oxides and the surface of the supports thus contributing to the increase in the dispersion of the oxides. However, in the case of TiMCM-41 containing catalyst the $NiMoO_4$ species are the most stabilized and thus leading to an increase in the catalytic activity of NiMo catalysts. Whereas the low activity of AlMCM-41 supported catalyst can be associated with too strong metal–support interaction (formation of $Al_2(MoO_4)_3$ and Ni distorted spinel-like structure) which in consequence inhibit the reduction and sulphidation of Ni and Mo species.
2. It was found that in the presence of the NiMo/SiMCM-41 and NiMo/TiMCM-41 catalysts the hydrogenation of DMBPh to MCHT occurs.
3. The molecular modelling shows that MoS_2/SiMCM-41 and MoS_2/AlMCM-41 display similar adsorptive properties with respect to both: 4,6-DMDBT and DMTHDBT. The incorporation of Ti atoms to the silica structure causes the increase of the adsorption of the intermediate with respect to the reactant, which suggests that competitive adsorption takes place. As the experiments of 4,6-DMDBT HDS show, the adsorption of the reactants does not have the crucial influence on the HDS efficiency via hydrogenation route, that it is overshadowed by the other factors – most probably this would be due to the metal–support interactions.

Acknowledgement

This work was supported by the Ministry of Science and Higher Education, Poland (Grant T09B 112 26).

References

[1] R. Silva-Rodrigo, C. Calderon-Salas, J.A. Melo-Banda, J.M. Dominguez, A. Vazquez-Rodriguez, Catal. Today 98 (2004) 123.
[2] R. Wojcieszak, S. Monteverdi, M. Mercy, et al., Appl. Catal. A: Gen. 268 (2004) 241.
[3] K. Mrozińska, J.R. Grzechowiak, Polish J. Environ. Stud. 18 (2009) 155.
[4] K. Mrozińska, J. Grzechowiak, Stud. Surf. Sci. Catal. 158 (2005) 1565.
[5] J.R. Grzechowiak, K. Mrozińska, A. Masalska, J. Góralski, J. Rynkowski, W. Tylus, Catal. Today 114 (2006) 272.
[6] M. Kruk, M. Jaroniec, A. Sayari, Chem. Mater. 11 (1999) 492.
[7] J. Ramírez, R. Contreras, P. Castillo, et al., Appl. Catal. A: Gen. 197 (2000) 69.
[8] S. Damyanova, A. Spojakina, K. Jiratova, Appl. Catal. A: Gen. 125 (1995) 257.
[9] T. Klimova, L. Lizama, J.C. Amezcua, P. Roquero, E. Terres, J. Navarrete, J.M. Dominguez, Catal. Today 98 (2004) 141.
[10] T. Klimova, E. Rodríguez, M. Martínez, et al., Micropor. Mesopor. Mater. 44–45 (2001) 401.
[11] T. Klimova, J. Reyes, L.O. Gutiérrez, Appl. Catal. A: Gen. 335 (2008) 159.
[12] Y.V. Plyuto, I.V. Babich, I.V. Plyutob, A.D. Van Langeveld, J.A. Moulijn, Colloids Surf. A: Phys. Eng. A 125 (1997) 225.
[13] P. Salerno, S. Mendioroz, A. López Agudo, Appl. Catal. A: Gen. 259 (2004) 17.
[14] Z. Liu, Y. Chen, J. Catal. 177 (1998) 314.
[15] P. Torres-Mancera, J. Ramirez, R. Cuevas, A. Gutierrez-Alejandre, F. Murrieta, R. Luna, Catal. Today 107–108 (2005) 551.
[16] P. Michaud, J.L. Lemberton, G. Pérot, Appl. Catal. A: Gen. 169 (1998) 343.
[17] D. Frenkel, B. Smit, Understanding Molecular Simulation: From Algorithms to Applications, Academic Press, San Diego, 1996.